ARTICLE

BIOTECHNOLOGY and BIOENGINEERING

Mechanism of Product Inhibition for Cellobiohydrolase Cel7A During Hydrolysis of Insoluble Cellulose

Johan P. Olsen,[1] Kadri Alasepp,[1] Jeppe Kari,[1] Nicolaj Cruys-Bagger,[1,2] Kim Borch,[2] Peter Westh[1]

[1]Research Unit for Functional Biomaterials, Roskilde University, NSM, 1 Universitetsvej, Build. 28, DK-4000 Roskilde, Denmark; telephone: +45 4674 2879; fax: +45 4674 3011; e-mail: pwesth@ruc.dk

[2]Novozymes A/S, Bagsværd, Denmark

ABSTRACT: The cellobiohydrolase cellulase Cel7A is extensively utilized in industrial treatment of lignocellulosic biomass under conditions of high product concentrations, and better understanding of inhibition mechanisms appears central in attempts to improve the efficiency of this process. We have implemented an electrochemical biosensor assay for product inhibition studies of cellulases acting on their natural substrate, cellulose. Using this method we measured the hydrolytic rate of Cel7A as a function of both product (inhibitor) concentration and substrate load. This data enabled analyses along the lines of conventional enzyme kinetic theory. We found that the product cellobiose lowered the maximal rate without affecting the Michaelis constant, and this kinetic pattern could be rationalized by two fundamentally distinct molecular mechanisms. One was simple reversibility, that is, an increasing rate of the reverse reaction, lowering the net hydrolytic velocity as product concentrations increase. Strictly this is not a case of inhibition, as no catalytically inactive is formed. The other mechanism that matched the kinetic data was noncompetitive inhibition with an inhibition constant of $490 \pm 40\ \mu M$. Noncompetitive inhibition implies that the inhibitor binds with comparable strength to either free enzyme or an enzymesubstrate complex, that is, that association between enzyme and substrate has no effect on the binding of the inhibitor. This mechanism is rarely observed, but we argue, that the special architecture of Cel7A with numerous subsites for binding of both substrate and product could give rise to a true noncompetitive inhibition mechanism.

Biotechnol. Bioeng. 2016;113: 1178–1186.

KEYWORDS: enzyme kinetics; product inhibition; cellulase; cellobiohydrolase; biosensor

Introduction

There are essentially two reasons to conduct enzyme inhibition studies (Cornish-Bowden, 2012). One is to elucidate reaction mechanisms and the other is to assess the rate of the reaction at different concentrations of substrate and inhibitor. Both of these aspects appear relevant in the case of product inhibition of the cellobiohydrolase, Cel7A (EC 3.2.1.176), an enzyme that is extensively utilized for the industrial conversion of lignocellulosic biomass to soluble sugars. This so-called saccharification process is typically conducted under conditions of high product concentrations, and tools for assessment of the associated inhibition would be useful in attempts to optimize the process. On the mechanistic level, molecular origins of Cel7A's product inhibition remains controversial (Andric et al., 2010), and this uncertainty impedes engineering of variants that are less prone to inhibition. Such variants have been suggested on the basis of computational work (Bu et al., 2011; Silveira and Skaf, 2015), and most recently also produced by site directed mutagenesis (Atreya et al., 2015). This latter work confirmed that the predicted mutations alleviated product inhibition, but also found that this improvement was generally associated with reduced catalytic efficiency. Thus, it appears that a more detailed understanding of enzyme-product interactions remains essential for rational design of improved variants.

Cel7A predominantly uses a processive mechanism, in which cellobiose molecules are consecutively cleaved off a cellulose strand threaded through the enzyme's binding tunnel. The most studied Cel7A is from *Tricoderma reseei* (an anamorph of *Hypocrea jecorina*), and product inhibition of this enzyme was considered already in early works (Katz and Reese, 1968). Since then, product inhibition of Cel7A and related enzymes has been studied extensively, but results have been conflicting both with respect to the mechanism and degree of the inhibition (Andric et al., 2010; Bu et al., 2011; Teugjas and

Conflicts of interest: NCB and KB work at Novozymes, a major manufacturer of industrial enzymes. Other authors have declared no conflicts of interest.
Correspondence to: P. Westh
Contract grant sponsor: Danish Council for Strategic Research, Program Commission on Sustainable Energy and Environment
Contract grant number: 11-116772
Received 21 September 2015; Revision received 23 November 2015; Accepted 29 November 2015
Accepted manuscript online 4 December 2015;
Article first published online 28 January 2016 in Wiley Online Library (http://onlinelibrary.wiley.com/doi/10.1002/bit.25900/abstract).
DOI 10.1002/bit.25900

Valjamae, 2013). A part of this discrepancy simply reflects experimental issues. For example, many studies have used crude enzyme extracts or commercial blends with a number of cellulolytic components (Bezerra and Dias, 2005; Holtzapple et al., 1984), while others have used purified enzyme (Gruno et al., 2004; Murphy et al., 2013; Teugjas and Valjamae, 2013). Other limitations for direct comparisons may relate to differences in experimental temperature, duration of the hydrolysis experiment or the choice of substrate (Andric et al., 2010). Regarding the latter, hydrolysis of soluble substrate analogues (which is convenient to assay) tend to show much stronger product inhibition than hydrolysis of insoluble cellulose (Gruno et al., 2004; Teugjas and Valjamae, 2013), and cellulases appear more sensitive to product inhibition when acting on crystalline cellulose than its amorphous counterpart (Johnson et al., 1982). It seems likely, that inhibition on genuine biomass substrates will also differ from their pure cellulose counterparts, and for this reason efforts have been made to study the inhibition of cellulase cocktails acting on genuine biomass substrates (Kadam et al., 2004). However, as pointed out by Andric et al. (2010), composition and levels of accessible substrate vary significantly between different biomass substrates making it impossible to obtain universally valid parameters from studies with these substrates.

In addition to these practical and experimental limitations, analysis of product inhibition for cellulases is also challenged by more fundamental issues. In particular, it is not clear if or how conventional inhibition theory based on the Michaelis–Menten (MM) framework can be used for the heterogeneous catalysis performed by cellulases. We have previously argued that for short contact times, an MM-type description of cellulase-activity provides a useful tool for kinetic analyses (Cruys-Bagger et al., 2013; Praestgaard et al., 2011). One key proviso for this approach is that the substrate must be in excess with respect to the enzyme (Cornish-Bowden, 2012). This assumption ($[E] << [S]$) is used in all simple MM-theory, but in practice it can be hard to verify in the case of cellulases because a molar concentration of the insoluble substrate cannot be readily specified. However, excess of substrate can be corroborated experimentally if the hydrolytic rate scales proportionally with the enzyme concentration (Cruys-Bagger et al., 2013).

The classical approach to enzyme inhibition has essentially never been used for cellulases acting on their insoluble substrate. This approach, as described in any biochemistry textbook, involves interpretation, often based on Lineweaver-Burk- or Hanes plots, of a number of MM curves each of which is measured at a different (constant) inhibitor concentration. One important attempt to apply this approach for Cel7A was published very recently (Kuusk et al., 2015). While in this case experimental limitations prevented direct determination of how the product modified V_{max} and K_M, analysis of IC_{50} (the inhibitor concentration that reduces the activity by half) at different substrate loads provided evidence of a non-competitive inhibition mechanism (Kuusk et al., 2015). Another application of traditional inhibition theory was presented by Bezerra and co-workers (Bezerra and Dias, 2004; Bezerra et al., 2011). In this case, the relevant MM rate equations with inhibition were integrated and fitted to experimental progress curves. One limitation of this approach, however, seems to be that factors other than product inhibition are known to play a role in the gradual activity loss of cellulases (Bansal et al., 2009), and this could affect both mechanistic and quantitative conclusions when integrated rate equations are fitted to prolonged experiments. Product inhibition studies are also challenged by difficulties associated with measuring a small change in product concentrations against a high background of the product added as inhibitor. This problem and ways to circumvent it for cellulolytic enzymes was recently discussed in some detail by Teugjas and Valjamae (2013).

In the work presented here, we have addressed the issue by implementing a new assay based on a pyranose dehydrogenase (PDH, EC 1.1.99.29) amperometric biosensor (Cruys-Bagger et al., 2014). This sensor quantifies soluble sugars in real time over a wide concentration range, allowing direct measurements of the initial, quasi-steady state rate even in samples with a high background of product (i.e., inhibitor). We used the conventional MM approach to distinguish different inhibitory mechanisms, and in the following we report the results from such analyses.

Materials and Methods

Enzymes and Buffers

Chemicals were obtained from Sigma–Aldrich (St. Louis, MO) and at least of HPLC grade. A 50 mM sodium acetate buffer, pH 5.0 with 2 mM $CaCl_2$, was used throughout unless otherwise stated. Cellobiohydrolase Cel7A from *T. reesei* and Pyranose Dehydrogenase (PDH) from *Agaricus meleagris* were heterologously expressed and purified to a single band on an SDS gel and the absence of cellobiase activity in the Cel7A stock in was confirmed as lack of detectable activity against the chromogenic substrate analogue para-nitrophenyl-glucopyranoside (results not shown) as described elsewhere (Cruys-Bagger et al., 2014; Westh et al., 2014). Protein concentration was measured at 280 nm in a Nanodrop Spectrophotometer (Thermo Scientific) using a theoretical molar extinction coefficient (Gasteiger et al., 2005) of 86.7 and 67.8 $mM^{-1}\,cm^{-1}$ for Cel7A and PDH, respectively. Final stock concentration of was 74 μM for Cel7A and 67 μM for PDH.

Inhibition Measurements (Soluble Substrate Analog)

Activity of 200 nM Cel7A on seven concentrations (0.2–1.7 mM) of para-nitrophenyl-lactopyranoside (pNPL) were determined in the presence of 0, 100, and 250 μM cellobiose resulting in [E]:[I] ratios of several orders of magnitude. The reagents were mixed in a 96-well microtiter plate (Nunc, Thermo Fisher Scientific, Waltham, MA) to a final volume of 210 μL, sealed with adhesive plastic and incubated for 40 min at 25°C, 750 rpm in a thermomixer (Eppendorf, Hamburg, Germany). The reaction was quenched with 100 μL 0.5 M glycine, 2 mM EDTA, pH = 10, and the concentration of p-nitrophenol released by Cel7A was quantified by absorbance measurements at 405 nm (Spectramax I3 plate reader, Molecular Devices, Sunnyvale, CA) with reference to an eight points standard curve ranging from 0 to 70 μM p-nitrophenol dissolved in the same pH 5 acetate reaction buffer used throughout the experiment.

Inhibition Measurements (Insoluble Cellulose)

The rate of cellobiose production was measured with a PDH modified biosensor. Preparation of the mediator-mixed carbon

paste electrode followed previously published procedures (Cruys-Bagger et al., 2012, 2014) using 1,4-benzoquinone as mediator. The electrode was covered by a Nuclepore polycarbonate membrane (TrackEtch membrane from Whatmann, USA) with a pore size and -density of 15 nm and $1 \cdot 10^5\,cm^{-2}$, respectively. The functionalized PDH-enzyme oxidizes soluble sugars and the resulting signal is recorded as the current required to keep a constant potential of 0.5 V against a Ag|AgCl reference. Hydrolysis experiments were carried out at 25°C in a 5 mL, water-jacketed reaction cell with magnetic stirring. Avicel PH 101 (0.5–40 g/L) suspended in either buffer or cellobiose solution (100, 250, or 500 μM, several orders of magnitude in excess of the enzyme concentration) was stirred at 600 rpm and after a stable output from the biosensor had been reached, enzyme solution was injected to a final concentration of 400 nM from a Chemyx Fusion 100 syringe pump. Subsequently, the production of cellobiose by Cel7A was monitored for 10 min., and the quasi steady state rate was specified as the slope of a straight line fitted to the data between 300 and 500 s (see Kari et al., 2014). At the highest inhibitor concentrations, the data at low substrate load (1–1.5 g/L) was discarded due to low signal/noise ratio. In a separate series of experiments 1 g/L Avicel (in pure buffer) was added, respectively, 300, 400, and 500 nnM Cel7A to confirm proportionality between activity and enzyme concentration. As already mentioned, such proportionality was considered evidence that the substrate was in excess at the investigated conditions.

For every 2–3 measurements, the sensor was calibrated by five consecutive 10 μL injections of a 20 mM cellobiose standard into the reaction cell loaded with the same solvent as in the hydrolysis experiments (either pure buffer or the relevant cellobiose solution). In this case the final cellobiose concentration would amount to 200 μM plus the added background, and this was well above the concentrations produced by hydrolysis. More details about the calibration procedures and sensitivity of the biosensor may be found elsewhere (Cruys-Bagger et al., 2014).

Results and Discussion

Implementation of Biosensor Assay

The hydrolytic rate of Cel7A was measured using a PDH modified carbon paste electrode, the use of which is described in detail elsewhere (Cruys-Bagger et al., 2014). The key premise for applying this electrochemical method in product inhibition assays is that the dynamic range of the biosensor extends well beyond product concentrations that are examined (~500 μM in this case). We tested the linearity of the sensor response by consecutive injections of cellobiose in the reaction cell and as illustrated in the example in Figure 1, we found a nearly linear response up to at least 800 μM cellobiose. It appears in the figure that there was a small, but systematic deviation from linearity. This is expected as the sensor enzyme, PDH, will show normal saturation behavior according to the MM equation (black line). As K_M for PDH/cellobiose is about 7 mM (Sygmund et al., 2008), however, the signal in the sub-mM range is almost linear. We conclude that the PDH biosensor readily quantifies changes in cellobiose concentrations even at the highest background concentrations used here. To minimize the impact of sensor saturation we used linear five point calibrations including the relevant background concentration of cellobiose.

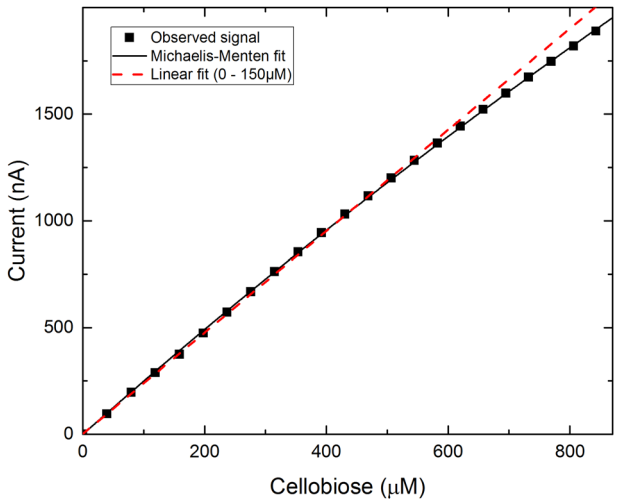

Figure 1. Calibration curve for a PDH sensor over the range used in this study. Raw biosensor output for incremental cellobiose concentrations (symbols) showed a small but systematic deviation from linearity (dashed line), but could be fitted to the Michaelis–Menten equation (full line). Even though all the data points were far below K_M, making this parameter difficult to assess, we found a K_M of approximately 7 mM in accordance with the literature value for PDH in solution (Sygmund et al. 2008). On a practical level the deviation from linearity was negligible compared to the experimental scatter in the investigated range (0–500 μM cellobiose).

As the measurements are performed in real time and the PDH-sensor showed a wide dynamic range, the signal resulting from added cellobiose can simply be zeroed out prior to enzyme injection, and changes in the concentration of soluble sugars due to the enzymatic reaction can subsequently be measured directly. This is illustrated in Figure 2, which shows results from four representative hydrolysis experiments. Enzyme was added at $t = 0$ and in some cases the raw signal (upper panel) only rose moderately over the background as the enzymatic reaction was started. However, when the constant background level was subtracted (lower panel) the activity of the enzyme can readily be singled out.

Cel7A Inhibition; Soluble Substrate

Inhibition of Cel7A by cellobiose was first measured during hydrolysis of the soluble substrate analog pNPL, and analyzed with respect to conventional theory (Cornish-Bowden, 2012; Segel, 1975). For simple systems, reversible inhibition may be generally described as illustrated in Scheme 1. We will only consider so-called linear inhibition where the product is solely formed by the reaction ES→E+P. Hyperbolic inhibition, that is, the situation where product may be formed directly from the ESI complex (EIS→EI+P), appears highly unlikely for Cel7A (*c.f.* Scheme 3 below) and will not be considered further.

The general case in Scheme 1, where the inhibitor has affinity for both E and ES, is known as mixed inhibition. In addition, there are three other special cases that characterize separate types of

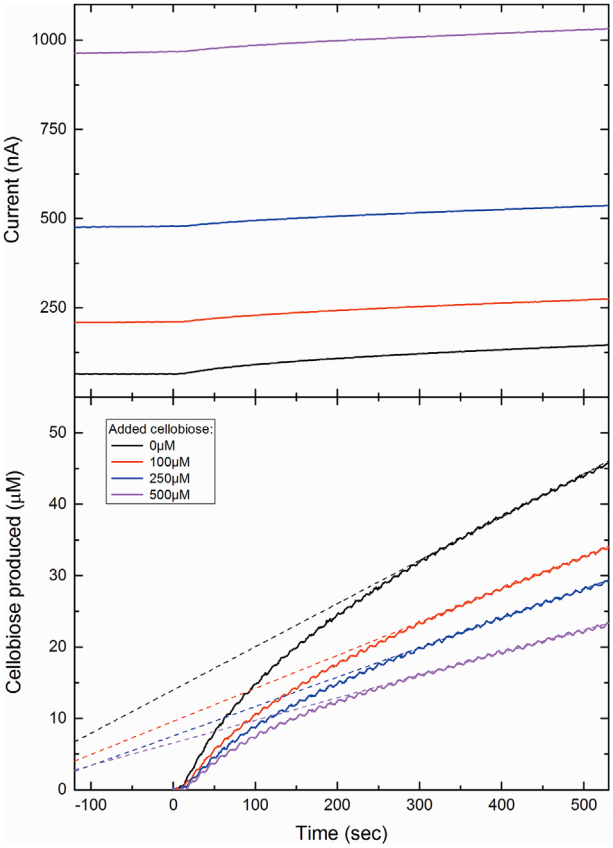

Figure 2. Examples of raw biosensor data (upper panel) and the determination of initial rates (lower panel) with increasing amounts of added cellobiose. Enzyme was injected at $t = 0$, and in some cases the sugar released by the enzymatic reaction only made a mode rate contribution to the total signal. In the lower panel, the signal has been corrected for background cellobiose and converted to concentration units on the basis of calibrations conducted with the relevant background. The initial quasi steady state rate was approximated as the slope of a line (dashed) fitted to the data after the burst phase (i.e., between $t = 300$ and $t = 500$ s, c.f. (Cruys-Bagger et al. 2013).

inhibition. The most important, competitive inhibition is the limiting case where the inhibitor binds to free enzyme (E), but not (or insignificantly) to the ES complex. This corresponds to $\alpha >> 1$ in Scheme 1; that is, that the dissociation constant for the ESI

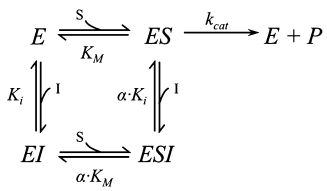

Scheme 1. Generalized reaction scheme for the effect of an inhibitor, I, on a simple enzyme reaction. K_M and K_i are the dissociation constants for the ES and EI complexes, respectively. The two other dissociation constants are αK_M and αK_i as specified in the scheme (α is a dimensionless constant). This simplification can be made because the product of the two equilibrium constants leading from E to ESI must be the same along each of the two possible paths (i.e., E→ES→ESI and E→EI→ESI, respectively).

complex (αK_i) is much larger than the dissociation constant of the EI complex (K_i). The opposite limiting case, un-competitive inhibition, is when the inhibitor solely binds to ES (i.e., $\alpha << 1$), and the situation between these two extremes, where $\alpha = 1$ is known as non-competitive inhibition (sometimes called true non-competitive inhibition to emphasize the difference from irreversible inhibition that shows the same kinetic hallmarks).

The kinetic equation for Scheme 1 under the usual quasi steady state assumption is quite complex with terms of both $[S]^2$ and $[I]^2$ (Cornish-Bowden, 2012) and therefore rarely used. Instead, a kinetic equation can readily be derived based on the rapid equilibrium assumption. The rate, $v = \mathrm{d[P]/dt}$, may be written

$$v = \frac{V_{\max} \cdot S_0}{\gamma_c \cdot K_M + \gamma_{uc} \cdot S_0} \tag{1}$$

In eq. (1) V_{max} has its usual meaning and K_M is the dissociation constant for the ES complex as illustrated in Scheme 1. We note, that in some works the dissociation constant (which is not strictly the same as the Michaelis constant K_M, derived for quasi steady state) is denoted K_S. However we will consistently use K_M in this work. The two other parameters in eq. (1) are defined

$$\gamma_c = 1 + \frac{[I]}{K_i} \tag{2}$$

$$\gamma_{uc} = 1 + \frac{[I]}{\alpha K_i} \tag{3}$$

Inhibition mechanisms are identified by analyzing experimental data with respect to eqs. (1–3). This has often been done by different linearized versions of eq. (1), but here we used a non-linear regression routine (OriginPro 2015, OriginLab Corporation Northampton, MA) and performed global analysis for the entire data set (i.e., hydrolytic rates as a function of $[S]$ and $[I]$). To discriminate between the inhibition mechanisms, separate regressions were performed with each of the four constraints: $\gamma_{uc} = 1$ (corresponding to competitive inhibition), $\gamma_c = 1$ (uncompetitive inhibition), $\gamma_c = \gamma_{uc}$ (non-competitive inhibition) and no constraints (mixed inhibition). To assess which of the four mechanisms best described the experimental data, we used the small-sample corrected Akaike Information Criterion (Akpa and Unuabonah, 2011; Kletting et al., 2009). This principle ranks different regressions of the same dataset on the basis of the residual sum of squares, the number of parameters and the number of data points. Specifically, we calculated the so-called Akaike weight, w_i, which provides an estimate of the validity of one model relative to the others. We note that this procedure of restrained global analyses and Akaike weight scores serves the same purpose as visual inspection of linearized expressions such as Hanes-, Lineweaver-Burk- or Dixon plots, which have been used extensively in the past. However, linearization may be statistically biased (Dowd and Riggs, 1965; Segel, 1975; Wilkinson, 1961), and we hence prefer to analyze the raw data without any preceding transformations. Moreover, nonlinear regression can be conducted globally over the $v([S],[I])$ plane, and hence without any requirement of constant inhibitor concentration for each MM-curve (this assumption is used in linearized analysis). This is an important advantage in the current work, as it allowed us to account for

the small increase in inhibitor (product) concentration, which inevitably occurred during the measurements.

Experimental data and global non-linear regression result for pNPL hydrolysis are shown in the left panel of Figure 3. It appears that cellobiose strongly inhibits the activity of Cel7A and regression analysis revealed that the competitive inhibition model provided by far the best account of the data ($w_i = 66\%$), with the maximum likelihood parameters shown in Table I. The inhibition constant K_i was 19 ± 0.3 μM. Un-competitive and non-competitive inhibition could not reproduce the data at all ($w_i = 0$), but the results could be reasonably described by mixed inhibition ($w_i = 34\%$). This latter analysis found one inhibition constant, K_i, which was identical to the the constant found in the competitive model (19 ± 0.6 μM), and another, much higher constant of $1{,}200 \pm 900$ μM (so α as defined in Scheme 1 was approximately 63). This higher K_i may reflect weak association in the binding tunnel, but the affinity of I for ES is very small compared to its affinity for the free enzyme, E, and the ability of the mixed model to account for the data is merely a slight modification of the comparative mechanism, which identifies an unimportant interaction of I and ES. Neglecting this, we arrive at the conclusion that the inhibition relies on the mutual (exclusive) competition of cellobiose and pNPL for the active site of Cel7A, and this competitive mechanism corroborates earlier studies using soluble substrate analogs (Teugjas and Valjamae, 2013; Vantilbeurgh and Claeyssens, 1985; von Ossowski et al., 2003). The value of K_i also matches dissociation constants found in cellobiose-Cel7A binding studies (Claeyssens et al., 1989; Colussi et al., 2015) as would be expected for a competitive inhibitor.

Inhibition; Insoluble Substrate

The quasi steady state rate for Cel7A hydrolyzing Avicel was measured with the biosensor as a function of both substrate load and concentration of cellobiose. The latter was determined as the mean concentration of cellobiose during the 200 s of data used for linear regression in Figure 2. Analysis of the surface regression in Figure 4 showed that a non-competitive mechanism accounted very well for the data ($w_i = 78\%$). The inhibition constant was 490 ± 40 μM ($\alpha = 1$ for non-competitive inhibition so this K_i is the apparent dissociation constant for both the EI and EIS complexes, c.f. Scheme 1). The analysis ruled out competitive- and uncompetitive mechanisms ($w_i \sim 0$), but found a moderate likelihood of mixed inhibition ($w_i = 21\%$). However, as the two inhibition constants derived from the regression in the mixed model were indistinguishable (440 ± 180 and 500 ± 60 μM) and equal to the value found in the non-competitive fit this result was in practice another demonstration of a non-competitive mechanism. Regression parameters from the mixed- and non-competitive models were self-consistent in the sense that K_M (1.8 g/L) and V_{max} (65 nM/s) were identical in the two analyses.

Insertion of $\alpha = 1$ (and hence $\gamma_{uc} = \gamma_c$) in eq. (1) shows that a non-competitive inhibitor reduces the maximal rate to the apparent value $V_{max}^{app} = V_{max}/\gamma_C$ while K_M remains unchanged. These changes in kinetic parameters would also occur if a fraction of the enzyme was irreversibly inactivated, and it has been claimed that reported cases of non-competitive inhibition may in fact often represent a misinterpretation of enzyme instability

Table I. Maximum likelihood parameters from the non-linear regression analyses. All measurements were conducted at pH 5.0 and 25°C.

Substrate	V_{max}/E_0 (min^{-1})	K_M	K_i (μM)	Inhibition type
pNPL	4.8 ± 0.002	0.7 ± 0.01 mM	18.7 ± 0.3	Competitive
Avicel	12 ± 0.24	1.8 ± 0.1 g/L	490 ± 40	Non-competitive

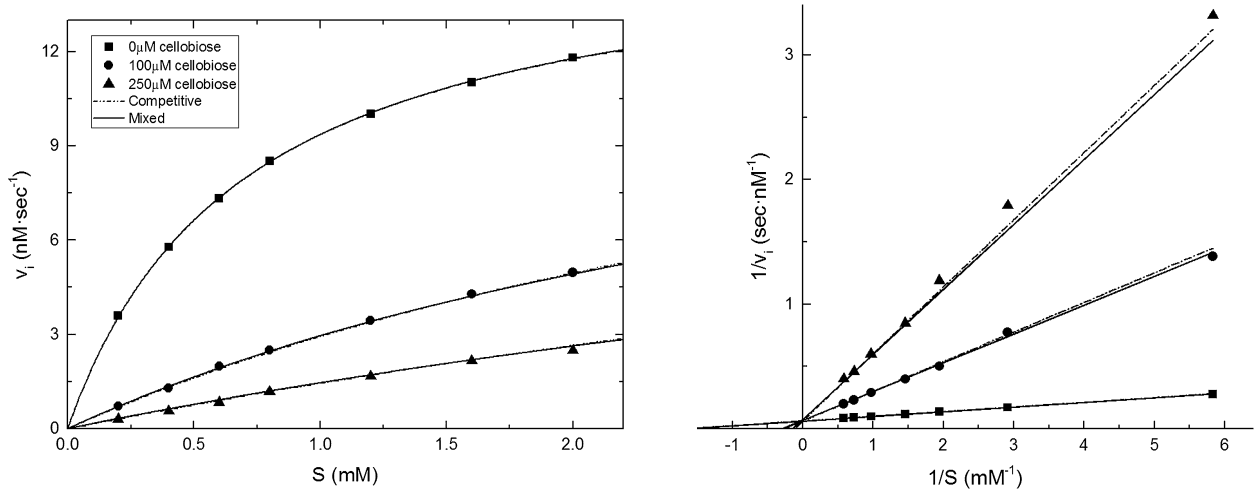

Figure 3. Left panel: Initial reaction rate for the hydrolysis of pNPL by Cel7A at different cellobiose concentrations. Symbols show raw data and lines are the results from the global, non-linear regression analysis of eq. (1). Right panel: Lineweaver-Burk plot (an often-used diagnostic plot for determining inhibition mechanism) of the same data also showing, that competitive (dashed line) and mixed (solid line) inhibition accounts well for the data. The lines are drawn with the regression parameters obtained from the non-linear regression in left panel.

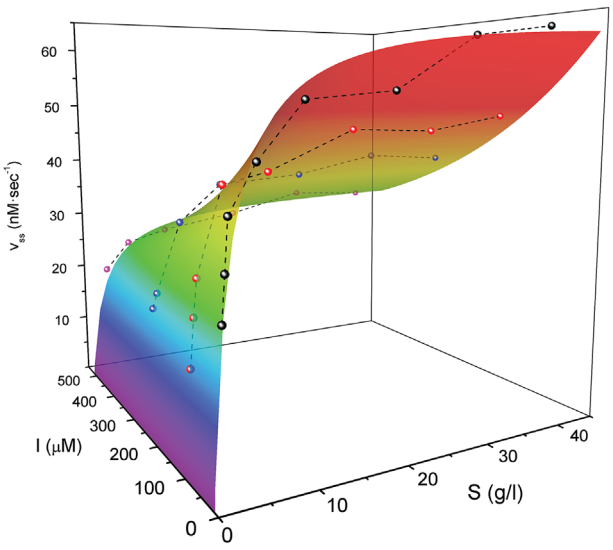

Figure 4. Balls represent quasi steady state rates determined as illustrated in Figure 2 with 0 μM (black), 100 μM (red), 250 μM (blue) and 500 μM (magenta) cellobiose added to the reaction mixture. The plot is analogous to the left panel of Figure 3 but with [I] as an independent variable instead of a fixed value. Surface represents best fit of eq. (1) with $\alpha = 1$, corresponding to non-competitive inhibition.

(Cornish-Bowden, 2012). For the current system, however, earlier work has demonstrated a negligible degree of inactivation at room temperature even in experiments extending for days (Alasepp et al., 2014), and it appears safe to rule out the influence of enzyme inactivation on the data in Figure 4, which are determined after a few minutes contact time (Fig. 2). Interestingly, a recent analysis of product (chitobiose) inhibition of a processive chitinase hydrolyzing insoluble (radioactively labeled) chitin (Kuusk et al., 2015) also suggested a noncompetitive mechanism with the same K_i value (450 μM) as found for cellobiose/Cel7A in the current work.

Turning to the molecular mechanism of the inhibition we note that a true non-competitive inhibitor as defined in Scheme 1 reduces the catalytic efficacy (V_{max}) without affecting the enzyme's affinity for the substrate. It has been claimed that this behavior is very rare (Segel, 1975) except perhaps for very small ligands such as protons, and even suggested that noncompetitive inhibition is "a phenomenon found mainly in textbooks" (Cornish-Bowden, 2012). Below we argue that the special architecture of Cel7A, with several pyranose binding sites both before and after the scissile bond might in fact lead to true non-competitive inhibition. First, however, we note that the most common reason for observing reduced V_{max} and unchanged K_M in the presence of product is simple reversibility of the enzyme reaction (Cornish-Bowden, 2012; Segel, 1975). We emphasize that inhibition and reversibility represent two fundamentally different mechanisms. In the case of inhibition, the rate is reduced as non-reactive enzyme complexes accumulate whereas reversibility lowers the net rate because the reverse reaction picks up speed as product accumulates. Ultimately, at equilibrium, the unidirectional rates become equal and the net rate is zero. We have previously argued (Praestgaard et al., 2011) that the mechanism of Cel7A (like many other hydrolytic enzymes) may be described as an ordered uni-bi reaction.[1] The processive mechanism for Cel7A complicates the steady state kinetic treatment (Cruys-Bagger et al., 2013), but if for simplicity we neglect processivity we may express the reaction as in Scheme 2. Here,

$$E + C_m \underset{k_{-1}}{\overset{k_1}{\rightleftharpoons}} EC_m \underset{k_{-2}}{\overset{k_2}{\rightleftharpoons}} EC_{m-2} + G_2 \underset{k_{-3}}{\overset{k_3}{\rightleftharpoons}} E + C_{m-2}$$

Scheme 2. Reaction scheme illustrating a simplified reversible degradation of substrate (C_m) by an enzyme (E) providing a possible interpretation of the observation that V_{max} was lowered while K_M was unchanged in the presence of product (G_2).

C_m represents the substrate, a cellulose strand with m glucose units. Upon hydrolysis, a cellobiose molecule, G_2, is first released from the complex which subsequently dissociates into the free enzyme, E, and a shortened cellulose strand, C_{m-2}. Reactions like the one in Scheme 2 have been systematically analyzed and the steady state rate equation in the presence of the first product, G_2, may be written

$$v = \frac{V_{max} C_m}{K_{M,1}\left(1 + \frac{K_{M,3}[G_2]}{K_{i,2}K_{M,2}}\right) + C_m\left(1 + \frac{[G_2]}{K_{i,1}}\right)} \qquad (4)$$

where the different K_M and K_i values are kinetic parameters defined from the rate constants in Scheme 2 (Segel, 1975). The exact definitions of these parameters can be found in the same reference, but for the current purpose, the main importance of eq. (4) is that it has the same mathematical form as eq. (1) (this can be seen by inserting eqs. (2–3) into eq. (1)). It follows that reversibility in Scheme 2 will have the same kinetic hallmarks as mixed inhibition, although no formal inhibition occurs (there is no non-reactive species), and we conclude that the kinetic effect of cellobiose on the activity of Cel7A illustrated in Figure 4 could in principle be explained by reversibility described by the reactions from right to left in Scheme 2.

In spite of the fact that reversibility is the most common reason for the type of kinetic behavior seen in Figure 4 (Cornish-Bowden, 2012), we suggest that a true non-competitive inhibition mechanism of Cel7A could be envisioned and perhaps provide a better explanation of the data. Thus, this otherwise rare mechanism could occur because Cel7A has a 50 Å long substrate binding tunnel with about 10 pyranose subsites. There are seven subsites (termed subsite −7 to −1) between the entry of the tunnel and the catalytic region, and two or three subsites (+1 to +3) near the exit, where the product is transiently located immediately after the glycosidic bond has been cleaved (Divne et al., 1998). It is well established that

[1] Strictly, the reaction is ordered bi-bi with the two substrates cellulose and water. Due to its high and hence constant concentration, water may be neglected in the kinetic treatment and the reaction can be described as ordered uni-bi.

cellobiose binds to the +1 to +2 subsites (sometimes called the expulsion site) in the absence of cellulose (Bu et al., 2011; Divne et al., 1998), and that the dissociation constant for this interaction is about 20 μM at room temperature (Claeyssens et al., 1989; Colussi et al., 2015) (this is the vertical equilibrium to the left in Scheme 3). It has also been shown that longer cello-oligosaccharides such as cellohexaose binds in the first part of the tunnel (subsite −7 to −2) (Divne et al., 1998) with a dissociation around 50 nM (Colussi et al., 2015). Conversely, filling the subsites near the scissile bond, particularly subsite −1, appears to be energetically unfavorable (Colussi et al., 2015), perhaps due to an associated strain in the pyranose ring (Knott et al., 2014). This is corroborated by structural evidence that longer oligosaccharides tend to occupy the beginning of the tunnel while the −1 site is largely unoccupied (Divne et al., 1998). Such a balance of strong attraction in each end of the tunnel and repulsion in the middle, suggests that intermediates with a product (cellobiose) in the expulsion site and/or a cellulose strand in the first part of the tunnel may be formed. This is illustrated in Scheme 3, which defines five enzyme species akin to those previously used by Väljamäe and co-workers to illustrate product inhibition of Cel7A (Gruno et al., 2004; Kuusk et al., 2015). In addition to the free enzyme (E), Scheme 3 defines complexes with product in the expulsion site (EP), substrate in the first part (possibly subsites −7 through −2) of the tunnel (ES) and a complex with both of these ligands (ESP). The last species in this scheme is the Michaelis complex (ES*), which has substrate filling the whole tunnel prior to catalysis.

If hydrolysis of the Michaelis complex is fast so that the population of ES* remains low, true noncompetitive inhibition could result from parallel and equal interactions of the E and ES states with cellobiose.

For the noncompetitive case ($\alpha \sim 1$) the inhibitor makes it appear as if less enzyme is present (reduced V_{max} and unchanged K_M). This apparent loss of enzyme may be quantified by the reaction rate at any given substrate load of an inhibited reaction v_{inh} relative to the uninhibited reaction, v_0. From eq. (1–3) we find that this ratio is

$$\frac{v_{inh}}{v_0} = \frac{\frac{V_{max} \cdot S_0}{\gamma \cdot (K_M + S_0)}}{\frac{V_{max} \cdot S_0}{K_M + S_0}} = \frac{1}{\gamma} = \frac{K_i}{[P] + K_i} \quad (5)$$

which corresponds to the remaining "active fraction" of enzyme $([E] + [ES])/E_0$ at product concentration [P] (Segel, 1975). Interestingly, this factor is independent of the substrate load, and the relative loss in activity is a simple function of the cellobiose concentration as expressed in eq. (5). Figure 5 shows v_{inh}/v_0 plotted against the cellobiose concentration for the current system. We suggest that due to the independence of substrate load, plots like this could be practical in assessments of product inhibition for Cel7A. We note, however, that the degree of inhibition is likely to depend on, for example, temperature and the physical properties of the insoluble substrate and a new plot like Figure 5 should therefore be made for the specific reaction conditions of interest. The approach in eq. (5) reiterates the fact that for non-competitive inhibition (unlike for other inhibition mechanisms) the often-reported parameter IC_{50} is equal to K_i (Cheng and Prusoff, 1973). This equality was utilized in a recent work on Cel7A product inhibition, which used highly crystalline (bacterial) cellulose as substrate (Kuusk et al., 2015). It was found that IC_{50} remained unchanged at different loads of substrate and hence also concluded that inhibition was best described by a noncompetitive mechanism

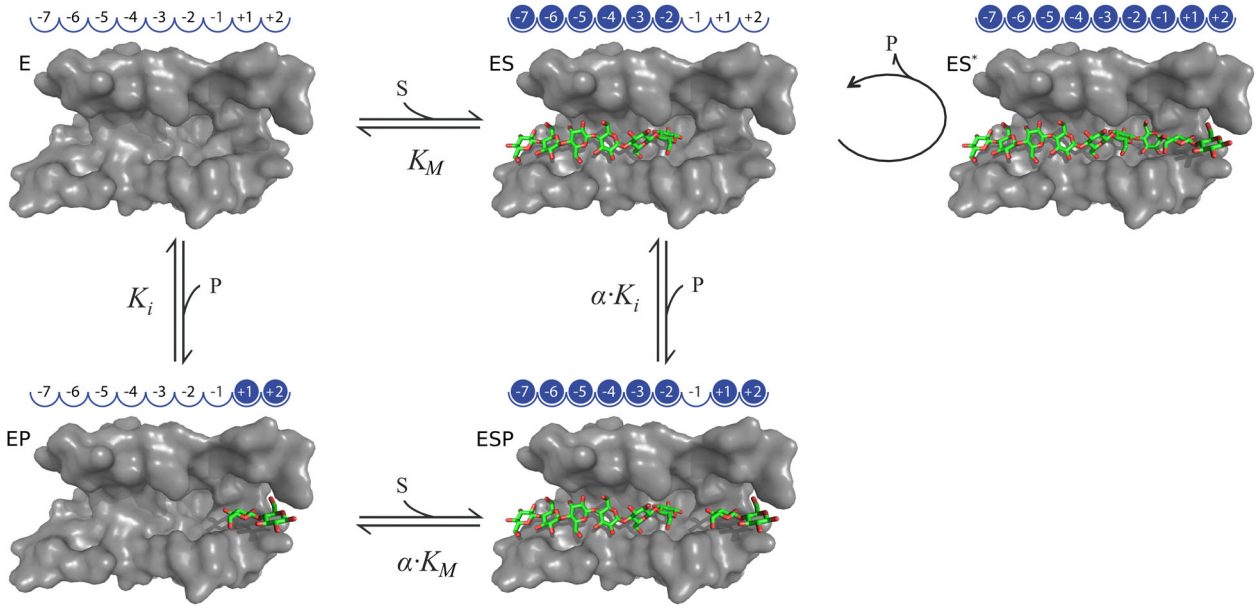

Scheme 3. Suggested structures underlying a true non-competitive inhibition mechanism for Cel7A. See text for detailed explanation. Enzyme (represented as the surface of tunnel-lining residues) with different ligands were derived from PDB entries 7CEL and 8CEL (Divne et al. 1998).

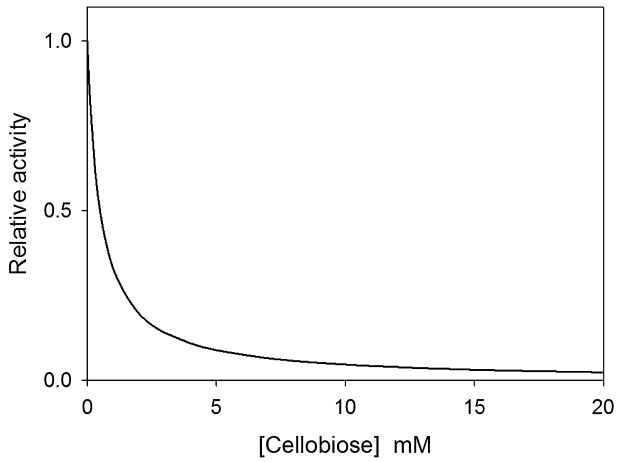

Figure 5. Relative activity of Cel7A against Avicel as a function of cellobiose concentration predicted by the K_i value obtained from Figure 4. For a noncompetitive inhibitor this fraction is independent of the substrate load.

with an inhibition constant of 170 ± 20 μM. This is in in reasonable accord with the K_i value found here particularly as crystallinity of Avicel is 0.5–0.6 compared to 0.76–0.95 for bacterial cellulose (Zhang and Lynd, 2004), and the strength of inhibition has been suggested to increase with substrate crystallinity (Johnson et al., 1982; Katz and Reese, 1968).

It is noticeable that the (non-competitive) inhibition constant found in Figure 4 ($K_i = 490$ μM) is much larger than the dissociation constant for the Cel7A-cellobiose complex (∼20 μM, see above). This disparity has been noted earlier (Kuusk et al., 2015) and it is in contrast to the results for the soluble substrate (Fig. 3), where the competitive inhibition constant found in the kinetic measurements matched the dissociation constant measured independently. This behavior is in fact expected for noncompetitive (and mixed) mechanisms. Thus, it most likely reflects that the four species in the circular reaction path of Scheme 3 (E, ES, ESP, and EP) are not at equilibrium. The lack of equilibrium in a circular reaction sequence at steady state is common due to the net flow through the cycle, and this is in contrast to "dead end" reactions such as the binding of a competitive inhibitor, which does not have a net flow and hence necessarily equilibrates, when the main reaction path is at steady state (Cornish-Bowden, 2012). Accordingly, we found $K_i = K_D$ for the competitive product inhibition of Cel7A during pNPL hydrolysis (Fig. 3), but not for the non-competitive inhibition mechanism on insoluble cellulose (Fig. 4). The lack of equilibrium in fact defies an important premise of eq. (1) as this was derived on under the rapid equilibrium approximation. Nevertheless, the current use of eq. (1) is common practice and preferred over the more complex steady-state solution of Scheme 1 as discussed above. The consequence of this is that for noncompetitive and mixed mechanisms, K_i values are not equilibrium constants, but mere kinetic parameters. This also implies that the observation of $\alpha = 1$ in Scheme 3 does not provide direct evidence that cellobiose has the same affinity for, respectively, E and ES (Scheme 3). To elucidate this question further, we measured the adsorption of Cel7A on Avicel with different background concentrations of cellobiose between 0 and 500 μM. In accordance with previous studies on isolated CBMs (Guo and Catchmark, 2013) the results (not shown) did not reveal systematic differences in enzyme adsorption, and this suggests that the EP complex (which dominates at high cellobiose concentrations) binds to Avicel with the same affinity as the free enzyme (which dominates in experiments with no added cellobiose). With respect to Scheme 3, this hints that the two horizontal equilibria have comparable dissociation constants. This, in turn, implies that α is around one and thus that cellobiose does appear to bind with equal strength to, respectively, E and ES. We note that this result could be considered in contrast with molecular dynamics simulations previously reported by Bu et al. (2012). What might seem like a discrepancy, however, could probably be explained by the fact that the authors did not include simulations where cellobiose was positioned in the so-called "primed state" (Knott et al., 2013). This alternate positioning of the cellobiose product, which is often observed in structures (Beckham et al., 2014), might lead to a simulation outcome in agreement with the results presented here, even though such simulations have not been reported to our knowledge. Based on previous thermodynamic (Colussi et al., 2015) and structural (Divne et al., 1998) studies, we suggest another possible explanation that, due to unfavorable interactions in the −1 site, this site might be largely unpopulated in the ES and ESP complexes. The associated spacing of cellulose and cellobiose could provide a possible explanation of our observation that the binding of cellobiose to the enzyme is unaffected by presence of a substrate chain in the binding tunnel. Thorough elucidation of this question is, however, beyond the current scope and will require an extended experimental material.

Conclusions

We have presented evidence that a PDH-biosensor can readily quantify initial quasi steady state rates of Cel7A even when product is added to the sample prior to the enzyme. This provides a convenient way to assess hydrolytic rates as a function of substrate- and product (i.e., inhibitor) concentrations, and hence to analyze product inhibition along the lines of traditional theories. We found that cellobiose reduced the maximal rate of Cel7A, while leaving K_M unaltered (Fig. 4), and concluded that this behavior could arise from two fundamentally different mechanisms namely simple reversibility (which is formally not a case of inhibition) or true non-competitive inhibition. Although true noncompetitive inhibition is rare in simple systems, we argue that it might well occur as the result of the special architecture of Cel7A (Scheme 3). Unlike the interpretation based on reversibility (Scheme 2) this latter suggestion (Scheme 3) accounts for the well-established binding of product to the free enzyme, and this may speak for noncompetitive inhibition as the most likely interpretation of the results. Simple inhibition studies, such as the current, cannot unambiguously distinguish between the two suggested interpretations. One way to achieve this distinction is by measurements of unidirectional reaction rates for example through the use of radioactively labelled material. We surmise that such work could further elucidate product effects on Cel7A activity and—on a more general level—contribute to the understanding of the activity loss or so-called slow-down, which appears to be ubiquitous for enzymatic hydrolysis of cellulose.

References

Akpa OM, Unuabonah EI. 2011. Small-Sample Corrected Akaike Information Criterion: An appropriate statistical tool for ranking of adsorption isotherm models. Desalination 272(1–3):20–26.

Alasepp K, Borch K, Cruys-Bagger N, Badino SF, Jensen K, Sørensen TH, Windahl MS, Westh P. 2014. In situ stability of substrate associated cellulases studied by scanning calorimetry. Langmuir 30:7134–7142.

Andric P, Meyer AS, Jensen PA, Dam-Johansen K. 2010. Reactor design for minimizing product inhibition during enzymatic lignocellulose hydrolysis: I. Significance and mechanism of cellobiose and glucose inhibition on cellulolytic enzymes. Biotechnol Adv 28(3):308–324.

Atreya ME, Strobel KL, Clark DS. 2015. Alleviating product inhibition in cellulase enzyme Cel7A. Biotechnol Bioeng. DOI: 10.1002/bit.25809

Bansal P, Hall M, Realff MJ, Lee JH, Bommarius AS. 2009. Modeling cellulase kinetics on lignocellulosic substrates. Biotechnol Adv 27(6):833–848.

Beckham GT, Ståhlberg J, Knott BC, Himmel ME, Crowley MF, Sandgren M, Sørlie M, Payne CM. 2014. Towards a molecular-level theory of carbohydrate processivity in glycoside hydrolases. Curr Opin Biotechnol 27:96–106.

Bezerra RMF, Dias AA. 2004. Discrimination among eight modified Michaelis-Menten kinetics models of cellulose hydrolysis with a large range of substrate/enzyme ratios. Appl Biochem Biotechnol 112(3):173–184.

Bezerra RMF, Dias AA. 2005. Enzymatic kinetic of cellulose hydrolysis—Inhibition by ethanol and cellobiose. Appl Biochem Biotechnol 126(1):49–59.

Bezerra RMF, Dias AA, Fraga I, Pereira AN. 2011. Cellulose hydrolysis by cellobiohydrolase Cel7A shows mixed hyperbolic product inhibition. Appl Biochem Biotechnol 165(1):178–189.

Bu L, Beckham GT, Shirts MR, Nimlos MR, Adney WS, Himmel ME, Crowley MF. 2011. Probing carbohydrate product expulsion from a processive cellulase with multiple absolute binding free energy methods. J Biol Chem 286 (20):18161–18169.

Bu L, Nimlos MR, Shirts MR, Ståhlberg J, Himmel ME, Crowley MF, Beckham GT. 2012. Product binding varies dramatically between processive and non-processive cellulase enzymes. J Biol Chem 287(29):24807–24813.

Cheng Y, Prusoff WH. 1973. Relationship between inhibition constant (K1) and concentration of inhibitor which causes 50 per cent inhibition (I50) of an enzymatic-reaction. Biochem Pharmacol 22(23):3099–3108.

Claeyssens M, Vantilbeurgh H, Tomme P, Wood TM, McRae SI. 1989. Fungal cellulase systems - comparison of the specificities of the cellobiohydrolases isolated from penicillium-pinophilum and trichoderma-reesei. Biochem J 261(3):819–825.

Colussi F, Sørensen TH, Alasepp K, Kari J, Cruys-Bagger N, Windahl MS, Olsen JP, Borch K, Westh P. 2015. Probing substrate interactions in the active tunnel of a catalytically deficient cellobiohydrolase (Cel7). J Biol Chem 290(4):2444–2454.

Cornish-Bowden A. 2012. Fundamentals of enzyme kinetics. Weinheim, Germany: Wiley-VCH.

Cruys-Bagger N, Badino SF, Tokin R, Gontsarik M, Fathalinejad S, Jensen K, Toscano MD, Sørensen TH, Borch K, Tatsumi H, Väljamäe P, Westh P. 2014. A pyranose dehydrogenase-based biosensor for kinetic analysis of enzymatic hydrolysis of cellulose by cellulases. Enzyme Microb Technol 68–4:58–59.

Cruys-Bagger N, Elmerdahl J, Praestgaard E, Borch K, Westh P. 2013. A steady-state theory for processive cellulases. FEBS J 280(16):3952–3961.

Cruys-Bagger N, Ren G, Tatsumi H, Baumann MJ, Spodsberg N, Andersen HD, Gorton L, Borch K, Westh P. 2012. An amperometric enzyme biosensor for real-time measurements of cellobiohydrolase activity on insoluble cellulose. Biotechnol Bioeng 109(12):3199–3204.

Divne C, Ståhlberg J, Teeri TT, Jones TA. 1998. High-resolution crystal structures reveal how a cellulose chain is bound in the 50 A long tunnel of cellobiohydrolase I from Trichoderma reesei. J Mol Biol 275(2):309–325.

Dowd JE, Riggs DS. 1965. A comparison of estimates of michaelis-menten kinetic constants from various linear transformations. J Biol Chem 240(2):863–869.

Gasteiger E, Hoogland C, Gattiker A, Duvaud S, Wilkins MR, Appel RD, Bairoch A. 2005. Protein identification and analysis tools on the ExPASy Server. In: Walker JM, editor. The proteomics protocols handbook. Totowa, New Jersey: Humana Press. p 571–607.

Gruno M, Väljamäe P, Pettersson Gr, Johansson G. 2004. Inhibition of theTrichoderma reesei cellulases by cellobiose is strongly dependent on the nature of the substrate. Biotechnol Bioeng 86(5):503–511.

Guo J, Catchmark JM. 2013. Binding specificity and thermodynamics of Cellulose-binding modules from trichoderma reesei Cel7A and Cel6A. Biomacromolecules 14(5):1268–1277.

Holtzapple MT, Caram HS, Humphrey AE. 1984. Determining the inhibition constants in the hch-1 model of cellulose hydrolysis. Biotechnol Bioeng 26(7):753–757.

Johnson EA, Reese ET, Demain AL. 1982. Inhibition of *Clostridium thermocellum* cellulase by end products of cellulolysis. J Appl Biochem 4:64–71.

Kadam KL, Rydholm EC, McMillan JD. 2004. Development and validation of a kinetic model for enzymatic saccharification of lignocellulosic biomass. Biotechnol Prog 20(3):698–705.

Kari J, Olsen J, Borch K, Cruys-Bagger N, Jensen K, Westh P. 2014. Kinetics of cellobiohydrolase (Cel7A) variants with lowered substrate affinity. J Biol Chem 289(47):32459–32468.

Katz M, Reese ET. 1968. Production of glucose by enzymatic hydrolysis of cellulose. Appl Microbiol 16(2):419–420.

Kletting P, Kull T, Reske SN, Glatting G. 2009. Comparing time activity curves using the Akaike information criterion. Phys Med Biol 54(21):N501–N507.

Knott BC, Crowley MF, Himmel ME, Stahlberg J, Beckham GT. 2014. Carbohydrate-protein interactions that drive processive polysaccharide translocation in enzymes revealed from a computational study of cellobiohydrolase processivity. J Am Chem Soc 136(24):8810–8819.

Knott BC, Haddad Momeni M, Crowley MF, MacKenzie LF, Götz AW, Sandgren M, Withers SG, Staìšhlberg J, Beckham GT. 2013. The mechanism of cellulose hydrolysis by a two-step, retaining cellobiohydrolase elucidated by structural and transition path sampling studies. J Am Chem Soc 136:321–329.

Kuusk S, Sørlie M, Väljamäe P. 2015. The predominant molecular state of bound enzyme determines the strength and type of product inhibition in the hydrolysis of recalcitrant polysaccharides by processive enzymes. J Biol Chem 290(18): 11678–11691.

Murphy L, Bohlin C, Baumann MJ, Olsen SN, Sorensen TH, Anderson L, Borch K, Westh P. 2013. Product inhibition of five Hypocrea jecorina cellulases. Enzyme Microb Technol 52(3):163–169.

Praestgaard E, Elmerdahl J, Murphy L, Nymand S, McFarland KC, Borch K, Westh P. 2011. A kinetic model for the burst phase of processive cellulases. FEBS J 278(9):1547–1560.

Segel IH. 1975. Enzyme kinetics: Behavior and analysis og rapid equilibrium and steady-state enzyme systems. New York: John Wiley & Sons Inc.

Sygmund C, Kittl R, Volc J, Halada P, Kubatova E, Haltrich D, Peterbauer CK. 2008. Characterization of pyranose dehydrogenase from Agaricus meleagris and its application in the C-2 specific conversion of D-galactose. J Biotechnol 133(3):334–342.

Teugjas H, Valjamae P. 2013. Product inhibition of cellulases studied with 14C-labeled cellulose substrates. Biotechnol Biofuels 6(1):104.

Vantilbeurgh H, Claeyssens M. 1985. Detection and differentiation of cellulase components using low-molecular mass fluorogenic substrates. FEBS Lett 187(2):283–288.

von Ossowski I, Stahlberg J, Koivula A, Piens K, Becker D, Boer H, Harle R, Harris M, Divne C, Mahdi S, et al. 2003. Engineering the exo-loop of Trichoderma reesei cellobiohydrolase, Ce17A. A comparison with Phanerochaete chrysosporium Cel7D. J Mol Biol 333(4):817–829.

Westh P, Kari J, Olsen JP, Borch K, Jensen K, Krogh KBRM. 2014. Cellobiohydrolase variants and polynucleotides encoding same.

Wilkinson G. 1961. Statistical estimations in enzyme kinetics. Biochem J 80(2): 324–332.

Zhang YHP, Lynd LR. 2004. Toward an aggregated understanding of enzymatic hydrolysis of cellulose: Noncomplexed cellulase systems. Biotechnol Bioeng 88(7):797–824.